Geophysical Research Letters

RESEARCH LETTER
10.1029/2018GL077427

Characterization of the Extraterrestrial Magnesium Source in the Atmosphere Using a Meteoric Ablation Simulator

D. L. Bones[1], J. C. Gómez Martín[1,2], J. D. Carrillo Sánchez[1], A. J. Dobson[1], and J. M. C. Plane[1]

[1]School of Chemistry, University of Leeds, Leeds, UK, [2]Instituto de Astrofísica de Andalucía (IAA-CSIC), Granada, Spain

Key Points:
- Differential ablation of Mg with respect to Na, Fe, and Ca observed from a range of meteoritic samples
- Experimental simulations confirm predictions of a chemical ablation model based on melt thermodynamics and Langmuir evaporation
- Mg should mostly ablate in the atmosphere between 80 and 90 km, with an ablation peak 4 km below that of Fe and 11 km below Na

Supporting Information:
- Supporting Information S1
- Movie S1
- Movie S2
- Movie S3
- Movie S4
- Movie S5
- Movie S6

Correspondence to:
J. M. C. Plane,
j.m.c.plane@leeds.ac.uk

Citation:
Bones, D. L., Gómez Martín, J. C., Carrillo Sánchez, J. D., Dobson, A. J., & Plane, J. M. C. (2018). Characterization of the extraterrestrial magnesium source in the atmosphere using a meteoric ablation simulator. *Geophysical Research Letters*, *45*. https://doi.org/10.1029/2018GL077427

Received 3 FEB 2018
Accepted 7 APR 2018
Accepted article online 19 APR 2018

Abstract Ablation of Mg from meteoroids entering the Earth's atmosphere was studied experimentally using a Meteoric Ablation Simulator: micron-sized particles of representative meteoritic material were flash heated to simulate atmospheric entry and the ablation rate of Mg with respect to Na measured by fast time-resolved laser-induced fluorescence. Over the range of particle diameters and entry velocities studied, Mg ablates 4.3 ± 2.1 times less efficiently than Na and 2.4 ± 0.8 times less efficiently than Fe. The resulting evaporation profiles indicate that Mg mostly ablates around 84 km in the atmosphere, compared with Fe at 88 km and Na at 95 km. The chemical ablation model Chemical Ablation Model predicts satisfactorily the measured peak ablation altitudes and relative ablated fractions of Mg, Na, Fe, and Ca but does not capture the breadth of the ablation profiles, probably due to the inhomogeneity of the minerals present in meteoroids combined with experimental limitations.

Plain Language Summary About 40 t of cosmic dust enters the Earth's atmosphere every day. These meteoroids, which contain minerals composed of metallic elements such as iron, sodium, calcium, and magnesium enter the Earth's atmosphere at high speeds (between 24,000 and 160,000 mph). The resulting flash heating caused by high-energy impacts with air molecules can lead to melting and in some cases complete evaporation of the particles—a process termed ablation. In this study, ablation is simulated using particles from different types of meteorite which are rapidly heated to well over 1700°C (3100°F) during the few seconds this would occur in the atmosphere. Lasers probe the resulting evaporation of a variety of metals. Here we show that magnesium evaporates less efficiently and at lower altitudes than sodium and iron, which is consistent with the predicted thermodynamics of the molten particles.

1. Introduction

A variety of metals, including Mg, ablate from particles (micron- to millimeter-sized meteoroids) during their entry into the Earth's atmosphere (Plane, 2012). This process produces layers of metal atoms and ions in the mesosphere and lower thermosphere (MLT) between 80 and 120 km (Plane et al., 2015). The metal atoms and ions undergo cycles of chemical reactions with gas phase constituents in the MLT (primarily O_3, O, H, O_2, CO_2, and H_2O) (Plane et al., 2015). In order to assess the impact of this extraterrestrial input on atmospheric phenomena, it is necessary to quantify the total input of meteoric elements into the atmosphere (Plane, 2012). Recent estimates of both the total dust input and the ablated elemental input (Carrillo-Sánchez et al., 2015, 2016) have combined size and velocity distributions of interplanetary dust derived from astronomical modeling of the Zodiacal Cloud (Nesvorný et al., 2010, 2011) with a detailed treatment of atmospheric entry and evaporation based on meteor physics and element-specific chemical ablation (Vondrak et al., 2008).

The ablation of meteoroids occurs largely due to evaporation from frictional heating (Vondrak et al., 2008). The degree of heating depends on the size, velocity and zenith entry angle of the incoming particle. For instance, a particle of 64-μm radius moving at 14 km s^{-1}, and entering at a zenith angle of 35°, will reach a temperature around 2300 K, hot enough to evaporate Mg. In order to provide an experimental benchmark for modeling meteoric ablation, we have constructed an experimental Meteoric Ablation Simulator (MASI) where micron-sized particles are heated under temperature profiles which mimic atmospheric ablation, while the evaporated metallic products are detected in real time (Bones et al., 2016). Previously, we have used the MASI to study the evaporation of Na, Fe, and Ca (Gómez-Martín et al., 2017). Ablation models, such as the Chemical Ablation Model (CABMOD) (Vondrak et al., 2008), have a number of important applications: calculating the injection profiles of different elements into the atmosphere required for atmospheric modeling (Carrillo-Sánchez et al., 2016; Plane, Feng, & Dawkins, 2015), determining the detection thresholds of

meteor head echoes by high-power and large-aperture radars (Janches et al., 2017), and interpreting the chemical fractionation (and depletion of volatiles) in cosmic spherules (Rudraswami et al., 2015).

This paper reports measurements of Mg evaporation profiles and ablated fractions as a function of particle mass and entry speed. Mg is the most abundant metal and the third most abundant element in carbonaceous Ivuna (CI) chondrites (Lodders, 2003), which are the closest in composition to interplanetary dust particles (IDPs; Jessberger et al., 2001). Mg exists mainly in the form of forsteritic olivine ($Mg_{2(1-x)}Fe_{2x}SiO_4$, where $x < 0.5$), which is the dominant mineral constituent of interplanetary dust and terrestrial meteorites (see section 2.2).

2. Methods

2.1. The Meteoric Ablation Simulator

The MASI has been described in detail previously (Bones et al., 2016; Gómez-Martín et al., 2017). Briefly, a small number of particles are placed on a tungsten ribbon that can be flash heated using a programmable power supply to simulate atmospheric heating of meteoroids. Size-segregated particle samples with a range of average radii (9–100 μm) are used, the upper limit constrained by the condition that the particles are small enough to be heated homogeneously (Bones et al., 2016). Heating profiles corresponding to each particle size for a range of entry velocities (14–31 km s^{-1}) and a zenith entry angle of 35° are programmed into the MASI. Two of the evaporating metals, in this case Na and Mg, are measured simultaneously by time-resolved laser-induced fluorescence (LIF). Each atmospheric profile simulation consists of a series of scans: first, an atmospheric heating profile (e.g., 2 s of heating to 2000 K); next, a gentle linear ramp from 1400 K up to 2700 K over 12 s, followed by a high-temperature "plateau" at 2700 K for about 10 s to remove any remaining Mg. These were followed by repeat blank scans of each temperature ramp. Separate sets of experiments were also run using only linear temperature ramps.

LIF was carried out with two 532 nm Neodymium-Yttrium Aluminum Garnet (Nd-YAG) lasers each pumping a Sirah Cobra dye laser, one operating at 10 Hz (Continuum Minilite) to detect Na (resonance transition 589.0 nm) and the other at 250 Hz (Litron) to detect Mg (resonance transition 285.2 nm). The fluorescence was collected through monochromators (10 nm bandwidth) and photomultiplier tubes orthogonal to the excitation beam. The temperature at the centre of the W ribbon was measured by a pyrometer (Land Instruments System 4, R1 ratio thermometer) with a time response of 15 ms. Temperature control and laser timings were achieved via a National Instruments Compact Rio Field Programmable Gate Array module running a custom built delay generator/proportional–integral–derivative (PID) control program. The pressure in the chamber was maintained at 15 Pa using a flow of N_2. A video camera mounted above the pyrometer captured videos of particles on the filament, with a frame rate of 20 Hz (see the supporting information Movies S1 to S6). Calibration scans were run with linear ramps using finely ground samples of the Chergach (H5) meteorite, with a known Mg:Na ratio of 16.7. These calibrations establish the relative intensities of the LIF signals with respect to the relative metal abundance. While the distribution of elements in meteorites on a submillimeter scale is highly variable, the finely ground sample gives a reasonable approximation to the bulk average, with each scan including approximately 50 to 100 particles.

2.2. Materials

Based on the elemental analysis of micrometeorites retrieved in the polar caps and interplanetary dust particles collected by aircraft in the stratosphere, the composition of interplanetary dust appears to be close to chondritic CI (Jessberger et al., 2001). The composition of cometary dust retrieved by the Stardust mission is consistent with that of Antarctic micrometeorites (Dobrica et al., 2009). Mineralogically, micrometeorites and IDPs appear to be closer to Carbonaceous Mighei (CM) chondrites (Rietmeijer, 2000). In practice, CI and CM meteorites are hard to obtain, while carbonaceous Vigarano (CV) and Karoonda (CK) meteorite fragments are more abundant due to several massive falls. The measurements reported here were conducted on Murchison (CM2 classification), Allende (CV3), and NWA5515 (CK4), as well as Chergach (H5—ordinary chondrite) for a reference. The amount of Murchison available was very small, limiting the number of measurements per atmospheric profile to two. Forsterite olivine ($Mg_{1.8}Fe_{0.2}SiO_4$) was also used as representative of the model composition considered in CABMOD, and as a contrast to the highly inhomogeneous meteoritic samples (Gómez-Martín et al., 2017), thus providing a diagnostic of potential experimental or modeling

shortcomings. The meteorite samples were ground into particles and then size sorted using mechanical dry sieving into four size bins with radii <19, 19–53, 53–75, 75–125 μm, within the IDP size range ($r < 200$ μm) that makes the largest contribution to the atmospheric input. The full width at half maximum (FWHM) of the measured size distributions of these bins was between 25 and 50 μm, while the mean radius of each size fraction agreed reasonably well with the nominal size defined by the sieves (Gómez-Martín et al., 2017). The number of particles deposited was typically 5–10 for the larger size bins and up to 100 particles for the smallest size bin. There is a balance between having small enough samples to avoid coalescence and having a representative composition. An analysis of Allende minerology based on Scanning electron microscope with energy-dispersive X-ray (SEM-EDX) data and Raman microscopy is included in the supporting information (Text S1 and Figures S6 and S7; Bonal et al., 2006; Kolesov & Tanskaya, 1996).

2.3. The CABMOD

CABMOD uses a multicomponent chemical equilibrium gas melt model known as MAGMA which calculates vapor pressures of components of a system of molten oxides, namely, Na_2O, K_2O, FeO, SiO_2, MgO, Al_2O_3, TiO_2, and CaO (Fegley & Cameron, 1987). MAGMA has been validated with experimental data of chemical fractionation in high-temperature melts (e.g., Hashimoto, 1983) over a wide range of temperatures and chemical compositions (Schaefer & Fegley, 2004). From the vapor pressures, the rate of evaporation for each species is calculated by assuming Langmuir evaporation, as expressed by the Hertz-Knudsen equation (Gómez-Martín et al., 2017; Vondrak et al., 2008). CABMOD computes the temperature change of the particle by considering the conservation of energy and momentum, which is iteratively calculated taking into account the rate of mass loss. The model therefore determines the evaporation rate of each element, as a function of altitude, from a meteoroid of specified initial mass, velocity, and entry angle (Carrillo-Sánchez et al., 2016).

3. Results and Discussion

3.1. Atmospheric Heating Profiles

Figure 1 shows time-resolved LIF profiles from evaporating Murchison meteorite particles, over a range of particle radii and simulated velocities (see also Figure S1 in the supporting information). Each panel depicts the average of two evaporation experiments on particles with a nominal size and velocity. The combinations of sizes and velocities were chosen to be appropriate to the meteoric input (Carrillo-Sánchez et al., 2016), although the range of combinations is limited by practical experimental considerations: the maximum particle size and velocity are constrained by the upper temperature limit of the pyrometer (2873 K). Figure 1 shows that larger, faster particles exhibit a greater extent of Mg evaporation. In all experiments except those simulating ablation of the very smallest and slowest particles (not included in Figures 1 and S1), all of the Na evaporates.

Evidence of particle melting is observed with the video camera images at around 1800 K, consistent with an overall olivine composition, although a significant amount of Na evaporates below this temperature. Clearly, most of the Na has evaporated before the Mg starts to evaporate. Previous experiments (Gómez-Martín et al., 2017; Hashimoto, 1983) and model calculations (Fegley & Cameron, 1987; Vondrak et al., 2008) indicate that K, Fe and Si also start evaporating ahead of Mg.

3.2. Linear Heating Ramp Profiles

It should be noted that the experimental evaporation profiles are only relevant if CABMOD correctly predicts the temperature profile on atmospheric entry, which depends on the mass loss of the particle, including the loss of Mg which is a major elemental constituent. Therefore, an independent test of CABMOD/MAGMA is necessary. This was achieved by applying linear temperature ramps to the meteoritic particles. The resulting profiles can then be compared with predictions of MAGMA under an identical temperature regime. Figure 2 presents a compilation of experiments run with linear temperature ramps. Here the particles were exposed to temperatures increasing from 1400 K to 2700 K at a rate of 120 K s^{-1}. Data from earlier evaporation experiments (Gómez-Martín et al., 2017) where Na, Fe, and Ca evaporation profiles were acquired are included in addition to Mg data from the present study. The evaporation profiles predicted by CABMOD for the linear temperature profile are also shown. For each set of experiments involving Na and one other metal, the profiles are normalized to the Na profile by the relative fractions ablated of Na and the second metal (see section 3.3). CABMOD satisfactorily predicts the temperature of maximum evaporation rate in the

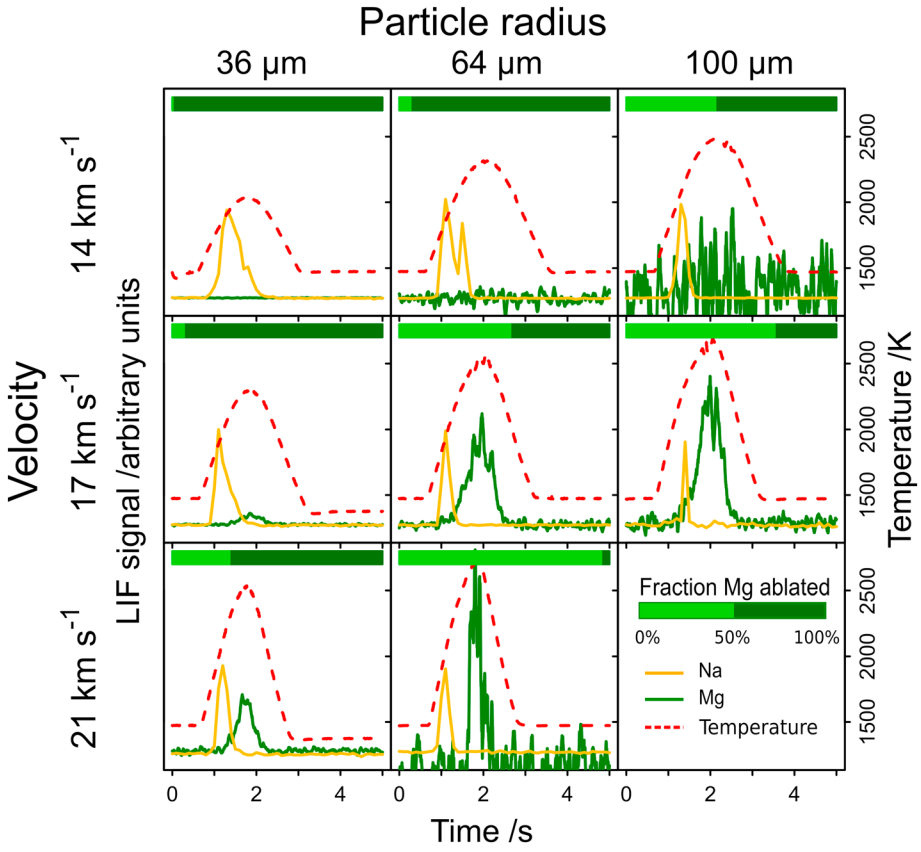

Figure 1. Atmospheric heating profiles applied to three different sizes of particles from the Murchison meteorite, simulated for three different entry velocities (entry zenith angle = 35°). The Na (orange line) and Mg (green line) laser-induced fluorescence profiles have been normalized to correspond to the evaporated fraction, based on the literature elemental composition of Murchison (Fuchs et al., 1973). The temperature profile is depicted with a dashed red line. The green bar at the top of each panel represents the fraction of Mg evaporated (light green bar) of the total (dark green is unevaporated Mg).

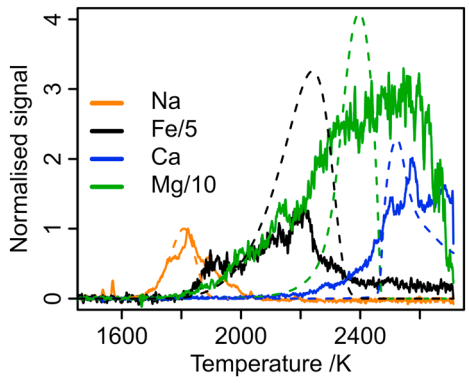

Figure 2. Normalized laser-induced fluorescence signals (solid lines) from Na, Fe, Ca, and Mg observed when a linear heating ramp (from 1400 K to 2700 K at a rate of 120 K s^{-1}) is applied to Allende meteoritic particles with a mean radius of 36 μm. The corresponding dashed lines show normalized Chemical Ablation Model simulations. Mg ablates at 2,475 ± 225 K in the experiment and at 2390 ± 70 K in Chemical Ablation Model.

evaporation profiles of each of the four metals. The onset of evaporation for the more volatile metals Na and Fe is also well captured. However, Fe and the more refractory metals—Mg and Ca—exhibit experimental profiles that are significantly broader than the CABMOD prediction. This is probably due primarily to the heterogeneity of the particles both in terms of composition and size and also in part to the temperature gradient on the filament. Where there are several particles present, with some a distance from the pyrometer focus, the temperature they experience can be significantly different. This issue is aggravated when the particles move on the filament as a result of electromigration (Bones et al., 2016).

Given that the nominal particle radius is actually the average of a size distribution, CABMOD was rerun assuming a realistic size distribution of particles (as measured by Gómez-Martín et al., 2017). This resulted in a broadening of the FWHM of the profile of about 20%. Forsterite experiments also showed considerable broadening (see Figure S5 in the supporting information). In the forsterite case, the broadening cannot be due to heterogeneities of composition, given that the samples are crystalline. A 20% broadening of forsterite evaporation peaks would result in profiles with a FWHM of about 180 K, applying the same linear

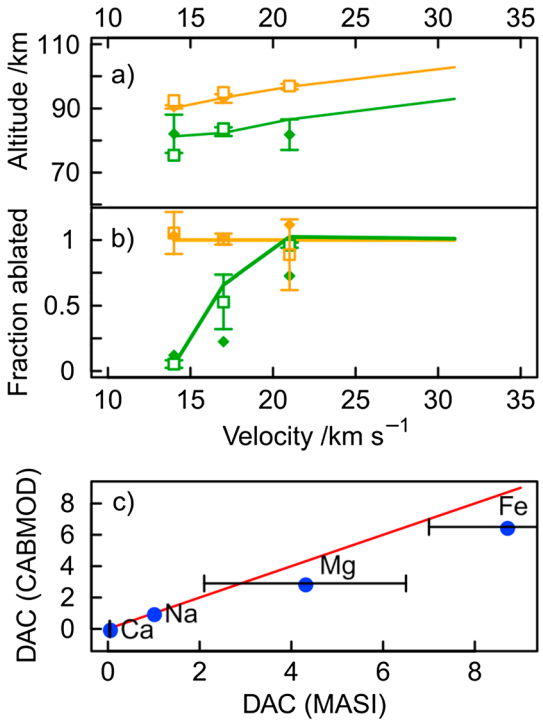

Figure 3. (a) The altitude of peak ablation for Na (orange) and Mg (green) predicted from Meteoric Ablation Simulator (MASI) measurements with Allende (filled diamonds) and Murchison (open triangles), compared with the Chemical Ablation Model (solid lines). Particle mean radius = 64 μm. (b) The fraction of Na and Mg evaporated, as a function of particle velocity for particles of mean radius = 64 μm (see also Figures S2 and S3 in the supporting information). (c) Comparison of the differential ablation coefficients (blue circles, normalized to Na) between MASI and Chemical Ablation Model; the red line is the 1:1 correspondence line. DAC = Differential ablation coefficients.

ramp. The actual profiles had a FWHM of around 300 K. Therefore, the majority of the broadening of the samples on the linear ramps is likely due to movement or variation in initial position and the resultant differences in temperature experienced by the particles on the filament (see Movie S5 in the supporting information). In contrast, the broadening of the Fe peak in forsterite is not as dramatic and the agreement with CABMOD is reasonably good. This is because Fe is more volatile and evaporates mainly when the particles are on the central part of the filament, where the temperature is close to the pyrometer reading.

For the majority of heating profiles with temperatures higher than 1900 K, the molten particles move along the filament during experimental runs due to the phenomenon of electromigration (Movies S1–S6 in the supporting information) (Bones et al., 2016; Kumar et al., 2014). The acceleration of the particles depends on the current flowing through the filament, so this effect is more pronounced at higher filament temperatures. This issue is less significant in the atmospheric evaporation profiles than the linear ramps, because the heating is more rapid and the particles do not have time to accelerate much before the filament is in the cooling phase. If the particles move during the subsequent high-temperature runs the fraction evaporated in the atmospheric profile will be overestimated. Figures 3b and S3 suggest that in comparison to CABMOD results, this does not result in a significant bias, but it may contribute to the large variability.

Given that the temperatures of maximum evaporation are well predicted by the model in the linear case, it is expected that the atmospheric temperature profiles from CABMOD that were used in the MASI simulations are close approximations to the actual temperatures experienced by meteoroids on atmospheric entry. One of the key predictions of CABMOD is the variation in the altitude of ablation for the different elements. For a particle of given composition, this altitude is governed primarily by temperature, which in turn depends on the initial velocity and the particle size. The Langmuir assumption—that the rate of evaporation is relative to the vapor pressure of individual species above the molten mixture—is seen to hold in terms of the order of evaporation and the relative amounts evaporated. Figure 3a illustrates the maximum altitude of ablation of Na and Mg as a function of particle velocity, for particles of mean radius = 36 μm. While the model and the experimental data diverge on the actual altitudes at high particle velocities, there is always a clear difference (~11 km) in maximum ablation altitude between the two metals.

3.3. Differential Ablation Coefficients

The differential ablation coefficient (DAC) is a useful measure of the relative ablation efficiencies of different meteoric elements. It is defined as the fraction evaporated of an element, Φ_M, divided by the fraction of sodium evaporated and multiplied by their relative elemental abundance in the particle before ablation:

$$\mathrm{DAC} = \frac{\Phi_\mathrm{M}}{\Phi_\mathrm{Na}} \times \frac{n_\mathrm{M}}{n_\mathrm{Na}} \quad (1)$$

where n_M is the relative abundance of element M in the meteoroid. The DAC values will therefore be specific to the meteoritic composition. For atmospheric modeling, a CI chondritic abundance would normally be used; here we convert the DAC of the meteorite samples into the corresponding CI chondrite DAC. Because of the varying ablation efficiency across the different size and velocity bins defined, the overall DAC of each element, as plotted in Figure 3c, is a weighted average of the DACs obtained using equation (1) for each combination of size and velocity (Gómez-Martín et al., 2017). The weighting factors are extracted from the velocity distribution of the Jupiter Family Comets and the size distribution derived from dynamical modeling of the Zodiacal Cloud constrained by observations by the Planck telescope (Table S1; Ade et al., 2014; Nesvorný et al., 2010, 2011). The CABMOD DAC for Mg is slightly lower than the MASI DAC; hence, it

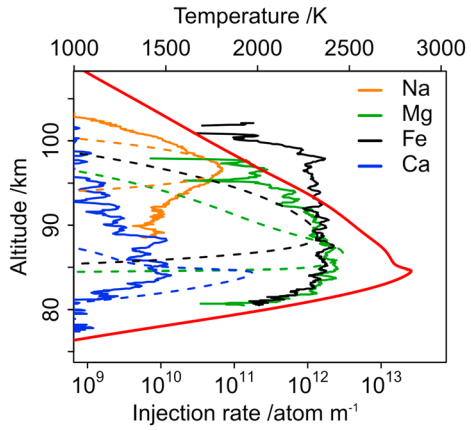

Figure 4. Elemental evaporation profiles for Na (orange), Fe (black), Mg (green), and Ca (blue), as predicted by Chemical Ablation Model (dotted line) and as measured by Meteoric Ablation Simulator (solid line). Temperature profile (experiment and model): Red solid line. Particle source: Allende meteorite, particle radius = 64 μm, velocity = 21 km s^{-1}. The data for Na, Fe, and Ca is taken from Gómez-Martín et al. (2017).

falls below the 1:1 correspondence line, as does the DAC of Fe. Overall, Fe ablated 2.4 ± 0.8 times more efficiently than Mg, resulting in Fe DAC values about twice those for Mg, since Mg is about 20% more abundant in CI chondrites. The MASI results show that Na ablates 4.3 ± 2.1 times more efficiently than Mg, compared with a CABMOD value of 6.2. CABMOD was run for each specific particle size and velocity and then the evaporated fractions were weighted by the size and velocity distributions, so that the DAC values plotted in Figure 3c are directly comparable with each other. Overall, the CABMOD predictions match the MASI data reasonably well, lending confidence in the atmospheric evaporation profiles produced by CABMOD. It should be noted that these DAC values are not necessarily representative of the actual meteoric input into the atmosphere, because only a subset of sizes and entry velocities were studied in the MASI; for calculations of the atmospheric meteoric input (using CABMOD) see the study by Carrillo-Sánchez et al. (2016).

3.4. Comparison of Modeled and Experimentally Simulated Atmospheric Profiles

Figure 4 displays atmospheric evaporation rate profiles of the four metals as a function of altitude for a specific particle size and velocity (radius = 64 μm, velocity = 21 km s^{-1}). The conversion of the MASI heating profile into altitude is described in Bones et al. (2016). The profiles have been normalized by area to the CABMOD Na profile, scaled by the experimentally determined DAC. Figure 4 shows that the experimentally derived altitude of maximum evaporation of each metal, as well as the relative rate of evaporation, are in good agreement with the CABMOD predictions. It is worth noting that CABMOD fails to replicate the width of the ablation profiles; the experimental profiles are significantly broader than those of the model. Table S2 lists the FWHMs of Fe, Mg, Ca, and Na for both the MASI experiments and CABMOD simulations. For this study, the MAGMA thermodynamic module in CABMOD assumes an essentially olivinic composition with a chondritic Fe:Mg ratio of 0.8 and a melting point of 1800 K (Vondrak et al., 2008). The melting point is represented within CABMOD by a sigmodal function which allows some spread of the melting point; some fraction of the particle melts ±100 K on either side of this melting point. However, this is unlikely to describe accurately enough the melting of multicomponent meteoroids. The olivine melting point ranges from 1500 K to 2150 K between pure fayalite (Fe_2SiO_4) and pure forsterite. The olivine particles sampled in the EDX measurements varied between Fo20 and Fo80 (where Fo*x* indicates that the sample is *x*% forsterite), which would still give a range of melting points of approximately 1550–2050 K.

Additionally, while olivine accounts for at least 50% of all the particles, several other minerals are present in significant fractions. The original analysis by Clarke et al. (1970) lists pyroxenes including enstatite, ferrosilite, and diopside as present in the matrix or chondrules of Allende. The point EDX analysis indicated that these compounds were all likely to be present, based on elemental ratios (see Text S1 in the supporting information). The assumption of a unique melting point for meteoroids based on an averaged olivine composition is currently made in CABMOD, but this does not capture the spread of melting points of the minerals in an actual meteoroid. Therefore, while the results from the linear ramps on forsterite suggest that a contribution to the profile broadening arises from the distribution and movement of particles on the filament such that they experience a range of temperatures, the inhomogeneity of the sample likely makes a significant contribution to the peak broadening.

4. Conclusions

The experimental simulations of the meteoric ablation of Mg demonstrate that this major metallic constituent is relatively refractory compared to Fe and particularly Na. Because the CI abundance of Mg relative to Fe is Mg/Fe = 1.2, the smaller DAC for Mg than for Fe implies that Mg ablates less efficiently, with Φ_{Fe}/Φ_{Mg} = 2.4 ± 0.8. Ablation is also "differential" in a spatial sense, since Mg mostly ablates around 84 km in the atmosphere, 4 km below Fe and 11 km below Na. The experimentally derived altitudes of peak ablation for the different metals, and their relative ablation efficiencies are satisfactorily predicted by the

ablation model CABMOD. However, CABMOD does not completely capture the evaporation of Mg because the element is not present as a single mineral phase in meteoroids: an ablating meteoroid will therefore melt inhomogeneously due to mineral phases with a range of melting points, resulting in the broader Mg (and Fe) ablation profiles measured by the MASI. Hence, the MASI results should be closer to the actual atmospheric situation.

Acknowledgments
This work was supported by the European Research Council (project 291332-CODITA). The MASI data and CABMOD output are archived at the Leeds University PETAL (PetaByte Environmental Tape Archive and Library; http://www.see.leeds.ac.uk/business-and-consultation/facilities/petabyte-environmental-tape-archive-and-library-petal/) and are available upon request to JMCP.

References

Ade, P. A. R., Planck Collaboration, Ade, P. A. R., Arnaud, M., Ashdown, M., Aumont, J., et al. (2014). Planck 2013 results. XIV. Consistency of the Planck data. *Astronomy and Astrophysics*, *571*, A14. https://doi.org/10.1051/0004-6361/201423743

Bonal, L., Quirico, E., Bourot-Denise, M., & Montagnac, G. (2006). Determination of the petrologic type of CV3 chondrites by Raman spectroscopy of included organic matter. *Geochimica et Cosmochimica Acta*, *70*(7), 1849–1863. https://doi.org/10.1016/j.gca.2005.12.004

Bones, D. L., Gómez-Martín, J. C., Empson, C. J., Carrillo-Sánchez, J. D., James, A. D., Conroy, T. P., & Plane, J. M. C. (2016). A novel instrument to measure differential ablation of meteorite samples and proxies: The Meteoric Ablation Simulator (MASI). *The Review of Scientific Instruments*, *87*(9), 094504. https://doi.org/10.1063/1.4962751

Carrillo-Sánchez, J. D., Nesvorný, D., Pokorný, P., Janches, D., & Plane, J. M. C. (2016). Sources of cosmic dust in the Earth's atmosphere. *Geophysical Research Letters*, *43*, 11,979–11,986. https://doi.org/10.1002/2016GL071697

Carrillo-Sánchez, J. D., Plane, J. M. C., Feng, W., Nesvorný, D., & Janches, D. (2015). On the size and velocity distribution of cosmic dust particles entering the atmosphere. *Geophysical Research Letters*, *42*, 6518–6525. https://doi.org/10.1002/2015GL065149

Clarke, R. S. J., Jarosewich, E., Mason, B., Nelen, J., Gómez, M., & Hyde, J. R. (1970). *The Allende, Mexico, meteorite shower*, *Smithsonian contributions to the Earth Sciences Smithsonian* No. 5. Washington, DC. https://doi.org/10.5479/si.00810274.5.1, 1, 53, 5.

Dobrica, E., Engrand, C., Duprat, J., Gounelle, M., Leroux, H., Quirico, E., & Rouzaud, J. N. (2009). Connection between micrometeorites and Wild 2 particles: From Antarctic snow to cometary ices. *Meteoritics and Planetary Science*, *44*(10), 1643–1661. https://doi.org/10.1111/j.1945-5100.2009.tb01196.x

Fegley, B., & Cameron, A. G. W. (1987). A vaporization model for iron silicate fractionation in the Mercury protoplanet. *Earth and Planetary Science Letters*, *82*(3–4), 207–222. https://doi.org/10.1016/0012-821x(87)90196-8

Fuchs, L. H., Olsen, E., & Jensen, K. J. (1973). *Mineralogy, mineral-chemistry, and composition of the Murchison (C_2) meteorite*. Washington DC: Smithsonian Institution Press. https://doi.org/10.5479/si.00810274.10.1, 10, 1, 39.

Gómez-Martín, J. C., Bones, D. L., Carrillo-Sánchez, J. D., James, A. D., Trigo-Rodriguez, J. M., Fegley, B., & Plane, J. M. C. (2017). Novel experimental simulations of the atmospheric injection of meteoric metals. *The Astrophysical Journal*, *836*(2), 212. https://doi.org/10.3847/1538-4357/aa5c8f

Hashimoto, A. (1983). Evaporation metamorphism in the early solar nebula—Evaporation experiments on the melt FeO-MgO-SiO_2-CaO-Al_2O_3 and chemical fractionations of primitive materials. *Geochemical Journal*, *17*(3), 111–145. https://doi.org/10.2343/geochemj.17.111

Janches, D., Swarnalingam, N., Carrillo-Sanchez, J. D., Gómez Martín, J. C., Marshall, R., Nesvorný, D., et al. (2017). Radar detectability studies of slow and small Zodiacal Dust Cloud Particles: III. The role of sodium and the Head Echo size on the probability of detection. *The Astrophysical Journal*, *843*(1), 1. https://doi.org/10.3847/1538-4357/aa775c

Jessberger, E. K., Stephan, T., Rost, D., Arndt, P., Maetz, M., Stadermann, F. J., et al. (2001). Properties of interplanetary dust: Information from collected samples. In E. Grün, B. S. Gustafson, S. Dermott, & H. Fechtig (Eds.), *Interplanetary dust* (pp. 253–294). Berlin, Heidelberg: Springer. https://doi.org/10.1007/978-3-642-56428-4_6

Kolesov, B. A., & Tanskaya, J. V. (1996). Raman spectra and cation distribution in the lattice of olivines. *Materials Research Bulletin*, *31*(8), 1035–1044. https://doi.org/10.1016/s0025-5408(96)00085-2

Kumar, P., Howarth, J., & Dutta, I. (2014). Electric current induced flow of liquid metals: Mechanism and substrate-surface effects. *Journal of Applied Physics*, *115*(4), 044915. https://doi.org/10.1063/1.4863641

Lodders, K. (2003). Solar system abundances and condensation temperatures of the elements. *The Astrophysical Journal*, *591*(2), 1220–1247. https://doi.org/10.1086/375492

Nesvorný, D., Janches, D., Vokrouhlický, D., Pokorný, P., Bottke, W. F., & Jenniskens, P. (2011). Dynamical model for the zodiacal cloud and sporadic meteors. *The Astrophysical Journal*, *743*(2), 129. https://doi.org/10.1088/0004-637x/743/2/129

Nesvorný, D., Jenniskens, P., Levison, H. F., Bottke, W. F., Vokrouhlický, D., & Gounelle, M. (2010). Cometary origin of the zodiacal cloud and carbonaceous micrometeorites. Implications for hot debris disks. *The Astrophysical Journal*, *713*(2), 816–836. https://doi.org/10.1088/0004-637x/713/2/816

Plane, J. M. C. (2012). Cosmic dust in the earth's atmosphere. *Chemical Society Reviews*, *41*(19), 6507–6518. https://doi.org/10.1039/c2cs35132c

Plane, J. M. C., Feng, W., & Dawkins, E. C. M. (2015). The mesosphere and metals: Chemistry and changes. *Chemical Reviews*, *115*(10), 4497–4541. https://doi.org/10.1021/cr500501m

Rietmeijer, F. J. M. (2000). Interrelationships among meteoric metals, meteors, interplanetary dust, micrometeorites, and meteorites. *Meteoritics and Planetary Science*, *35*(5), 1025–1041. https://doi.org/10.1111/j.1945-5100.2000.tb01490.x

Rudraswami, N. G., Prasad, M. S., Dey, S., Plane, J. M. C., Feng, W., & Taylor, S. (2015). Evaluating changes in the elemental composition of micrometeorites during entry into the Earth's atmosphere. *The Astrophysical Journal*, *814*(1). https://doi.org/10.1088/0004-637x/814/1/78

Schaefer, L., & Fegley, B. (2004). A thermodynamic model of high temperature lava vaporization on Io. *Icarus*, *169*(1), 216–241. https://doi.org/10.1016/j.icarus.2003.08.023

Vondrak, T., Plane, J. M. C., Broadley, S., & Janches, D. (2008). A chemical model of meteoric ablation. *Atmospheric Chemistry and Physics*, *8*(23), 7015–7031. https://doi.org/10.5194/acp-8-7015-2008